Smectic Ordering in Main-Chain Siloxane Polymers and Elastomers Containing *p*-Phenylene Terephthalate Mesogens

Harshad P. Patil, Jian Liao, and Ronald C. Hedden*

Department of Materials Science and Engineering, The Pennsylvania State University, University Park, Pennsylvania 16802

Received March 15, 2007; Revised Manuscript Received June 21, 2007

ABSTRACT: Main-chain liquid crystalline polymers that form low-temperature smectic mesophases are prepared by linking terephthalic acid, bis(4-allyloxyphenyl) ester (PPT) mesogens with 1,1,3,3,5,5-hexamethyltrisiloxane (F3) spacers via Pt-catalyzed hydrosilylation. Significant differences in thermal behavior and mesomorphic ordering are found between the polymer having unsubstituted PPT mesogens (F3-PPT-H) and the polymer having methyl substituents on the terminal rings of the mesogens (F3-PPT-CH_3). Combined evidence from polarized light optical microscopy, differential scanning calorimetry, and X-ray diffraction reveals S_{CA} ordering in both polymers. Smectic elastomers are prepared by nonlinear polymerization of PPT-H or PPT-CH_3 mesogens with F3 spacers and a tetrafunctional cross-linker, tetrakis(dimethylsiloxy)silane (A_4). The dynamic mechanical response of unoriented, polydomain elastomers is characterized in small-strain, oscillatory shear. A prominent peak in tan δ ($\equiv G''(\omega)/G'(\omega)$) associated with the smectic−isotropic clearing transition dominates the mechanical loss spectrum. Mesogen ring substitution is a simple synthetic approach to tuning the dynamic mechanical response of smectic elastomers for possible applications in vibration isolation or impact absorption.

1. Introduction

Thermotropic main-chain liquid crystalline polymers (MCLCP) are semiflexible macromolecules having rigid structural units (mesogens) embedded in their backbones, which encourages formation of one or more stable mesophases. Linear MCLCP[1] and cross-linked elastomers (MCLCE)[2] combine the chainlike architecture of polymers with the inherent anisotropy of liquid crystals, leading to striking rheological or mechanical phenomena. LCE of both the side-chain and main-chain type have generated interest for their exceptional vibration damping characteristics[3,4] and as soft actuators with properties that potentially mimic the characteristics of muscle tissue.[5−8] Compared to LCE of the side-chain type, MCLCE have more direct coupling between mesogen orientation and polymer backbone conformation and therefore potentially exhibit stronger deviations from ordinary rubber elasticity.

MCLCP and MCLCE based upon mesogens connected by highly flexible oligodimethylsiloxane units are widely studied for their easily accessible, low-temperature mesophases.[9−17] Previous studies of polysiloxane MCLCP and MCLCE examined mesogens of the 1,4-bis(benzoyl)hydroquinone (BHQ) type,[9,10,18] 1-biphenyl-2-phenylbutane type,[3,19,20] or others.[21] On the other hand, no reports have examined polysiloxane MCLCP or MCLCE based upon the *p*-phenylene terephthalate (PPT) type of mesogen,[11] which have been used to prepare main-chain LC polyesters with alkyl spacers[22] and densely cross-linked thermosets.[23] PPT mesogens differ from the BHQ type in the reversal of the ester bridges, which one might expect to stiffen the polymer backbone and thereby raise the temperature range of mesophase stability. However, comparing model compounds or polyesters having BHQ or PPT type mesogens, the PPT compounds often exhibit similar clearing temperatures.[24,25] Thus, polysiloxanes with PPT mesogens should also exhibit low-temperature mesophases, but no study of their synthesis and properties has appeared.

* Corresponding author: Tel 814-863-2325; fax 814-865-2917; e-mail hedden@matse.psu.edu.

We therefore examined thermal behavior and mesomorphic ordering in two linear polymers consisting of PPT mesogens connected by flexible hexamethyltrisiloxane (F3) spacers, which are shown to form S_{CA} mesophases based on evidence from polarized light optical microscopy and X-ray diffraction. We also examine smectic ordering in MCLCE prepared from PPT mesogens by a one-step, nonlinear polycondensation of mesogen, F3 spacers, and a tetrafunctional A_4 siloxane cross-linker, tetrakis(dimethylsiloxy)silane. Addition of methyl ring substituents to the terminal aromatic rings of the mesogens dramatically impacts the clearing transition temperature and therefore significantly impacts the rheological or dynamic mechanical behavior of the linear polymers and elastomers. Smectic MCLCE prepared from PPT mesogens exhibit high mechanical damping associated with the clearing transition, which can be manipulated by varying the ring substituents of the mesogens, suggesting possible use as "tunable" vibration damping elastomers.

2. Experimental Section

2.1. Materials. 2-Methylhydroquinone (99%), allyl bromide (99%), terephthalic acid (98+%), 4-(dimethylamino)pyridine (DMAP) (99%), sodium hydride (60% oil dispersion), and *N*,*N*′-dicyclohexylcarbodiimide (DCC) (99%) were purchased from Alfa Aesar. Anhydrous sodium sulfate (99%), dimethyl sulfoxide (DMSO) (99.8%), and dichloromethane (99.5%) were obtained from EMD Chemicals. Hydroquinone (99%) and terephthaloyl chloride were purchased from TCI America. 1,1,3,3,5,5-Hexamethyltrisiloxane (F3) (99%) and tetrakis(dimethylsiloxy)silane (A_4) were purchased from Gelest, Inc. Materials were used as received.

2.2. Mesogen Syntheses. Two different synthetic routes were followed in preparing PPT mesogens (Figure 1). Synthesis of PPT-H followed route 1. Synthesis of PPT-CH_3 followed route 2, producing a mixture of products with structural isomerism in the placement of $-CH_3$ groups on the terminal aromatic rings.

2.2.1. Synthesis of 4-Allyloxyphenol. Hydroquinone (11.0 g, 100 mmol) was dissolved in 100 mL of DMSO in a three-neck round-bottom flask under a nitrogen flow in a water bath at ambient temperature. NaH (4.00 g, 100 mmol, 60 mass % oil immersion)

10.1021/ma0706374 CCC: $37.00
Published on Web 07/28/2007

Route 1.

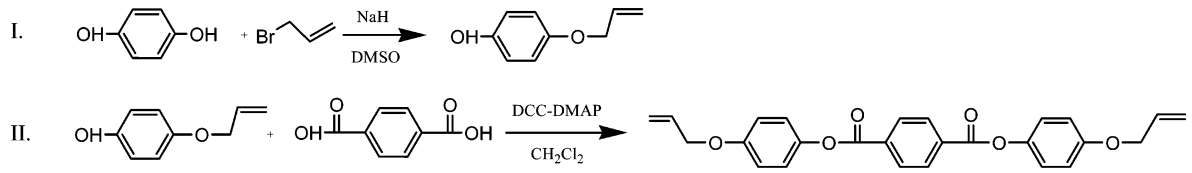

Route 2.

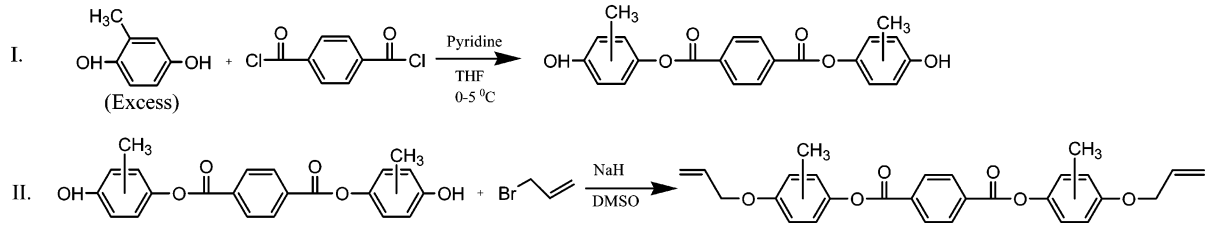

Figure 1. Synthesis of allyloxy-terminated PPT-H and PPT-CH_3 mesogens.

was added gradually over ~100 min to the solution of hydroquinone and DMSO. Allyl bromide (12.1 g, 100 mmol) was added to the reaction mixture with a dropping funnel. The reaction was carried out for 4 h and was terminated by pouring the mixture into distilled water with stirring, after which the product was isolated by extraction with dichloromethane, dried over anhydrous Na_2SO_4, and then filtered. The solution was passed through a column packed with silica gel (Grade 9385, 230−400 mesh, 60 Å, Sigma-Aldrich) to remove the oil from the NaH dispersion and reaction byproducts. The product was isolated by rotary evaporation of CH_2Cl_2. The 4-allyloxyphenol (7.00 g, 47%) thus obtained was dried in vacuum overnight and further purified by column chromatography using ethyl acetate/hexane (1:2 v/v) as mobile phase. ^{1}H NMR (400 MHz; $CDCl_3$; $(CH_3)_4Si$): δ_H 4.51 (2H, $-CH_2$, d), 5.30 (1H, $-CH_2$, d), 5.39 (1H, $-CH_2$, d), 6.04 (1H, −CH, m), 6.77 (4H, aromatic, m).

2.2.2. Synthesis of Terephthalic Acid, Bis(4-allyloxyphenyl) Ester (PPT-H). 4-Allyloxyphenol (15.01 g, 100.0 mmol), DCC (20.63 g, 100.0 mmol), DMAP (1.22 g, 10.1 mmol), terephthalic acid (8.30 g, 50.0 mmol), and CH_2Cl_2 (150 mL) were homogenized by stirring and allowed to react for 48 h at room temperature. The reaction mixture was filtered and washed with 2.0 N aqueous HCl and dried once over anhydrous Na_2SO_4 and then passed through a silica gel column using dichloromethane as mobile phase to obtain purified PPT-H (yield = 49% based on terephthalic acid). ^{1}H NMR (300 MHz; $CDCl_3$; $(CH_3)_4Si$): δ_H 4.59 (4H, $-CH_2$, t), 5.34 (2H, $-CH_2$, d), 5.46 (2H, $-CH_2$, d), 6.08 (2H, −CH, m), 6.99 (4H, aromatic, d), 7.16 (4H, aromatic d), 8.36 (4H, aromatic s) ^{13}C NMR ($CDCl_3$, 400 MHz): δ_C 118.23 (***C***H_2=), 133.50 ($-CH_2-$***C***H=CH_2), 69.65 (−***C***H_2−CH=CH_2), 156.94 (***C*****$_{ar}$**$-OCH_2-CH=CH_2$), 115.88, 122.71 (***C*****$_{ar}$,** outer rings), 144.72 (***C*****$_{ar}$**−OCO−, outer rings), 165.02 ($C_{ar}-$***C***OO−), 134.34 (***C*****$_{ar}$**−COO−), 130.629 (***C*****$_{ar}$**−central ring). FT-IR (KBr disk, cm^{-1}): 2875, 2887 (C−H stretch), 3068 (=C−H stretch), 1652 (C=C stretch), 1512 (C=C aromatic stretch), 1730 (C=O stretch).

2.2.3. Synthesis of Bis(4-hydroxy-x-methylphenyl) Terephthalate (Mixed Isomers, x = 2 or 3). The synthetic route reported by Barclay et al.[23] was followed, except our product was purified by column chromatography using ethyl acetate as mobile phase (yield = 70% based on terepthaloyl chloride). ^{1}H NMR (300 MHz; $(CDCl_3)_2$; $(CH_3)_4Si$): δ_H 2.08, 2.15, and 2.24 (6H, $-CH_3$, mixture of isomers), 2.84 and 2.87 (2H, −OH, mixture of isomers), 6.76−7.05 (6H, aromatic, m), 8.33−8.38 (4H, aromatic, m).

2.2.4. Synthesis of Terephthalic Acid Bis(4-allyloxy-x-methylphenyl) Ester (Mixed Isomers, x = 2 or 3) (PPT-CH_3). 37.80 g (100.0 mmol) of bis(4-hydroxy-*x*-methylphenyl) terephthalate was dried in a vacuum oven at 45 °C and then dissolved in 300 mL of DMSO in a three-neck, 1000 mL round-bottom flask in a water bath held at ambient temperature. NaH (12.00 g) was added to the reaction mixture gradually over 100 min under nitrogen flow. After 90 additional min, 30.0 mL of allyl bromide (41.9 g, 347 mmol) was added to the mixture, after which the reaction proceeded for 4 h. The reaction was terminated by decanting into 1000 mL of distilled water with stirring, and the solid product was isolated by filtration. The product was dissolved in dichloromethane and was stirred with anhydrous Na_2SO_4 for 2 h, then filtered, and passed through a silica gel column using dichloromethane as mobile phase. PPT-CH_3 (14 g, 38%) thus obtained was recrystallized several times using ethyl acetate and hexanes. ^{1}H NMR (300 MHz; $CDCl_3$; $(CH_3)_4Si$): δ_H 2.24 (6H, $-CH_3$, m), 4.61 (4H, $-CH_2$, d), 5.32 (4H, $-CH_2$, d), 5.43 (4H, $-CH_2$, d), 6.08 (2H, −CH, m), 6.85 (4H, aromatic, m), 7.08 (4H, aromatic, m), 8.35 (4H, aromatic s). ^{13}C NMR ($CDCl_3$, 400 MHz): δ_C 117.54 (***C***H_2=), 134.27 ($-CH_2-$***C***H=CH_2), 69.84 (-***C***$H_2-CH=CH_2$), 165.15 ($C_{ar}-$***C***OO−), 134.49 (***C*****$_{ar}$**−COO−), 130.87 (***C*****$_{ar}$,** central ring), 143.43, 144.29 (***C*****$_{ar}$**−OCO−, outer rings), 155.12, 156.96 (***C*****$_{ar}$**$-OCH_2-CH=CH_2$), 112.26, 118.08, 122.76, 122.98, 124.16 (***C*****$_{ar}$**−outer rings), 16.92 ($C_{ar}-$***C***H_3). FT-IR (KBr disk, cm^{-1}): 2866, 2931 (C−H stretch), 1734 (C=O stretch), 3033 (=C−H stretch), 1494 (C=C aromatic), 1651 (C=C stretch).

2.3. Polymer Synthesis. Linear main-chain polymers were formed by an "$A_2 + B_2$" type polycondensation (Figure 2) with B_2 ≡ mesogen (allyloxy-functionalized) and A_2 ≡ 1,1,3,3,5,5-hexamethyltrisiloxane (F3) (silane-functionalized). The polycondensation was a standard Pt-catalyzed hydrosilylation in dichloromethane similar to that described by Mather et al. for synthesis of main-chain polysiloxanes with BHQ-type mesogens.[18] Step-growth polymerization was catalyzed by the platinum(0)−1,3-divinyl-1,1,3,3-tetramethyldisiloxane complex (Figure 2) at 45−50 °C for several days to 1 week. Polymers were subsequently fractionated at ambient temperature by dissolving in toluene (100 mL/1.0 g of polymer) in a 4 L Erlenmeyer flask and precipitating by slow addition of methanol with stirring. After addition of methanol, 2−3 days were allowed for the polymer-rich phase to collect at the bottom of the flask at room temperature. After removal of the polymer-rich phase, methanol addition was continued to obtain additional fractions, with a total of six fractions recovered. Roughly 5−15 mass % of the polymer was precipitated in each fraction. Properties of fractions used in the current study are summarized in Table 1. In all cases, M_w/M_n after fractionation (determined by SEC) was substantially less than the value of 2.0 expected for polycondensation. Fractions were dried under vacuum at 50 °C for 7 days before further analysis. Chemical structures of the fractionated linear polymers were verified by ^{1}H NMR using a Bruker DMX300 spectrometer (300 MHz; $CDCl_3$; $(CH_3)_4Si$).

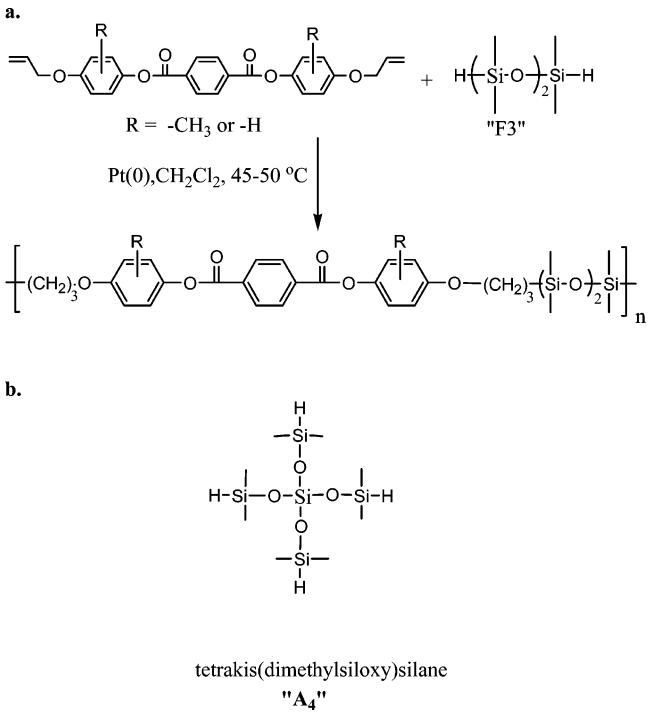

Figure 2. (a) Step-growth hydrosilylation reaction used to prepare linear polymers from allyloxy-terminated mesogens and flexible connectors. (b.) Structure of "A_4" cross-linker used in nonlinear polymerizations to prepare networks.

2.4. Elastomer Synthesis. Two MCLCE were prepared via a one-step, nonlinear polycondensation of mesogen (B_2), 1,1,3,3,5,5-hexamethyltrisiloxane (A_2), and tetrakis(dimethylsiloxy)silane (A_4), which is conceptually similar to an approach described by Finkelmann et al.[14] The mole fraction of A groups (SiH) belonging to cross-linkers is defined as

$$\rho \equiv \frac{\text{moles A groups belonging to branched monomers}}{\text{total moles A groups}} = \frac{4(\text{moles } A_4)}{2(\text{moles } A_2) + 4(\text{moles } A_4)} \quad (1)$$

and ρ was set to 0.08 for both elastomers. Monomers were dissolved in dichloromethane (1.0 mL CH_2Cl_2/1.0 mmol mesogen) at 45−50 °C and cross-linked for 7 days with 1.0 mass % of the Pt(0) catalyst. After 7 days of reaction, the dichloromethane was allowed to evaporate by air-drying. Reaction and drying proceeded in air for an additional 1 day and under vacuum for 1 day. The mole ratio of total A groups (SiH) to B groups (allyl) was calculated from

$$r = [4(\text{moles } A_4) + 2(\text{moles } A_2)]/[2(\text{moles } B_2)] \quad (2)$$

and r was varied systematically to identify "optimal" elastomers having the minimum degree of equilibrium swelling in toluene. An optimal value $r_{opt} = 1.50 \pm 0.05$ was used to prepare the elastomer containing PPT-H mesogens (E-H), and $r_{opt} = 1.36 \pm 0.05$ was used to prepare the elastomer containing PPT-CH_3 mesogens (E-CH_3). Observing $r_{opt} \neq 1.0$ is not unusual for hydrosilylation cross-linking. Substantial deviations from stoichiometric conditions have been previously observed in Pt-catalyzed hydrosilylation end-linking studies with A_4 cross-linker and B_2 = polydimethylsiloxane (PDMS)[26] or poly(diethylsiloxane) (PDES).[27] The origin of the deviation has been debated and appears to have more than one underlying cause.[26,28] "Optimal" elastomers E-H and E-CH_3 were extracted in toluene for 7 days to remove solubles, during which time the toluene was replaced with fresh solvent daily. Swollen elastomers were deswollen by slow addition of methanol (a poor solvent) to the toluene over a period of a few days, to avoid cracking from rapid evaporation of solvent, followed by air-drying and vacuum-drying at 50 °C, prior to characterization.

2.4. Size Exclusion Chromatography (SEC). Molar masses of the linear polymers were determined by size exclusion chromatography (SEC) using a Shimadzu system with a series of three columns (Styragel HR 7.8 × 300 mm columns with 5 μm bead size: 100−10 000, 500−30 000, and 5000−6 000 000 Da) from Polymer Laboratories, Inc., and both refractive index (RI) and ultraviolet absorption (UV, 254 nm) detectors. Measurements were performed in THF at 35 °C with a flow rate of 1 mL/min.

2.5. Polarized Light Optical Microscopy (POM). Samples were characterized via orthoscopic observation between crossed polarizers in an Olympus BX51 microscope with UMPlanFL 5×, 20×, or 100× objectives. Films of linear polymers (irregular thickness, typically 1−10 μm) were deposited on a glass slide by evaporation from a 1.0 mass % solution of acetone or dichloromethane. After air-drying, each sample was annealed on an Instec HS400 hot stage at a temperature (1−5 °C) above its clearing temperature for 12 h to ensure removal of residual solvent and then ramp-cooled at 2 °C/h until a well-defined optical texture was observed at a final temperature (quoted in text). No coverslips were used. In some cases, annealing was instead followed by quick cooling to a specific temperature (where indicated in text). Images were recorded using a 2.0 megapixel Diagnostic Instruments model 11.2 Color Mosaic digital camera equipped with Spot digital imaging software.

2.6. Differential Scanning Calorimetry (DSC). A Seiko Instruments DSC 220 CU equipped with a liquid nitrogen cooling tank was used to characterize thermal transitions in fractionated linear polymers. After crimping 3−7 mg of polymer into a TA Instruments aluminum pan, a standard thermal treatment was applied. Samples were first heated above their clearing (isotropization) temperatures to erase previous thermal history, then cooled quickly to 22 °C, and allowed to equilibrate for 3 days. DSC heating traces were recorded by initially cooling to −30 °C and then applying a heating ramp at 10 °C/min under a flowing N_2 atmosphere. Indium was used as a calibration standard for both the temperature and heat flow scales. Transition temperatures (T_2, T_i) reported were taken as the temperature at which the peak of the endotherm was observed at a heating rate of 10 °C/min; the uncertainty in the peak position was ±2 °C or less based upon multiple runs. DSC traces also exhibited the typical inflection associated with the glass transition (T_g), and values reported in Table 1 are based upon the midpoint of the inflection at the chosen heating rate.

2.6. Wide-Angle X-ray Diffraction (WAXD). Wide-angle X-ray diffraction (WAXD) experiments were performed on samples of 0.5−1 mm thickness in transmission using a Rigaku D/MAX Rapid II instrument equipped with graphite monochromator, 300 μm pinhole collimator, and Cu Kα source ($\lambda = 1.5418$ Å). Unoriented linear polymers were characterized in transmission after being subjected to the same thermal treatment as the samples studied by DSC. Corrections for polarization and oblique incidence were applied to raw data using Rigaku AreaMax software. No corrections were applied for background scattering or instrumental broadening.

Table 1. Molar Masses of Fractionated Linear Polymers, Values of T_g, T_2, and T_i Determined by DSC, and *d*-Spacings for Smectic Layering Reflection Determined by WAXD at 22 °C (Uncertainties Are Quoted in the Experimental Section)

polymer (fraction)	M_w (kg/mol)	M_w/M_n	T_g (°C)	T_2 (°C)	T_i (°C)	*d* (Å)
F3-PTP-H	85	1.4	8	52	130	28.0
F3-PTP-CH_3 (Fr. 2)	77	1.3	8	30	72	28.0
F3-PTP-CH_3 (Fr. 5)	11	1.1	8	*a*	72	28.0

[a] Not observed.

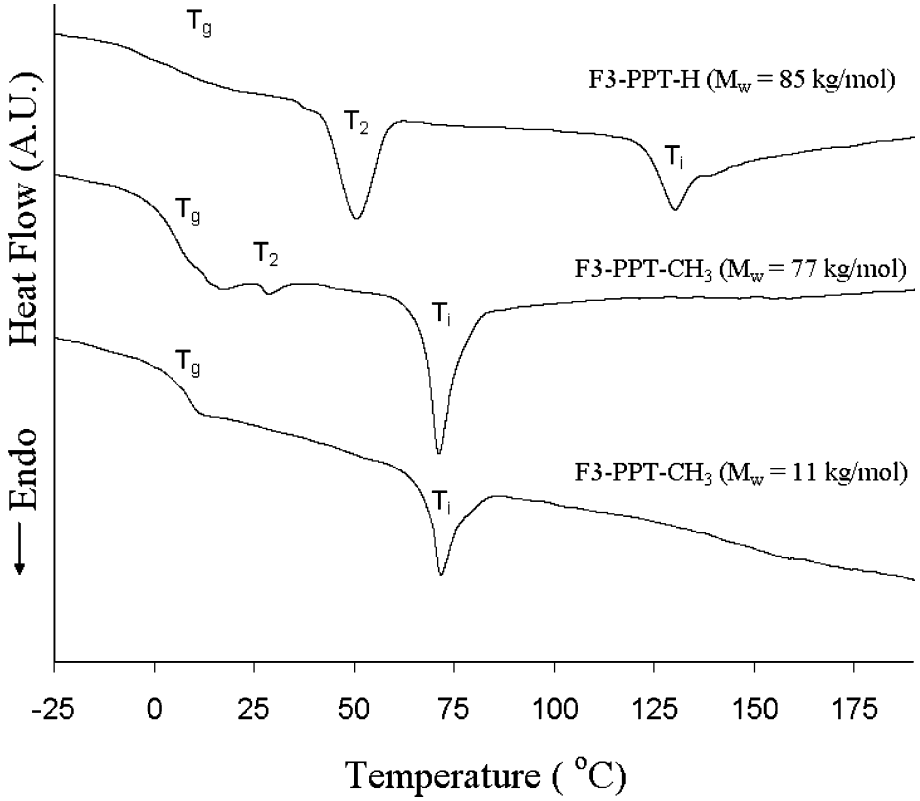

Figure 3. DSC heating traces for fractionated F3-PPT-H and F3-PPT-CH_3.

Diffractometer scans (intensity vs 2θ) were obtained by circular averaging of intensity over a range of ($2° \leq 2\theta \leq 30°$). Azimuthal scans (intensity vs χ) were recorded by averaging the diffracted intensity over a finite interval $\Delta(2\theta)$, which is specified for each sample in the relevant figure captions. Calculated *d*-spacings for smectic layering were estimated by applying the Bragg relationship ($n\lambda = 2d \sin \theta$) to the first order ($n = 1$) layering reflection, based upon the value of (2θ) at which peak intensity was observed. Experimental uncertainty in the calculated *d*-spacings is ±1.0 Å based upon observations from multiple measurements.

Diffraction patterns for oriented F3-PPT-CH_3 were obtained by drawing the sample at room temperature (22 °C). WAXD experiments were conducted immediately thereafter as well as 2 and 16 days after stretching. An additional WAXD pattern was obtained after heating this sample to 65 °C. Diffraction patterns for oriented F3-PPT-H were obtained after drawing the sample at 70 °C, allowing 10 min at 70 °C, and cooling to 22 °C. An additional WAXD pattern was obtained after reheating this sample to 100 °C. Diffraction patterns of oriented elastomers were obtained while subjecting the samples to uniaxial tension. The local extension ratio ($\lambda = L/L_0$) was determined by marking the elastomer surface with two small ink dots and comparing the final (L) and initial (L_0) lengths between dots by optical microscopy. Elastomer E-H was warmed to 70 °C in a water bath during drawing and then cooled to 22 °C under tension, whereas E-CH_3 was drawn at 22 °C. The incident X-ray beam was normal to the axis of extension for all oriented linear polymers and elastomers.

2.7. Dynamic Mechanical Analysis (DMA). Dynamic storage and loss moduli of extracted MCLCE were measured using a TA Instruments Q800 DMA with the shear sandwich fixture. Samples were cut from a flat sheet of approximate thickness 0.5 mm that had been cured in a flat-bottom poly(tetrafluoroethylene) (PTFE) vial. Storage and loss moduli were measured at a small strain amplitude ($\gamma_0 = 0.005$) using an isothermal frequency sweep, which was repeated at temperatures separated by 5 °C intervals.

3. Results and Discussion

3.1. Linear Polymers. Figure 3 presents DSC heating traces for F3-PPT-H and two samples of F3-PPT-CH_3 of differing molar mass. In each trace, the endotherm designated T_i is the clearing temperature (liquid crystalline to isotropic transition). The second endotherm at lower temperature (designated T_2) is due to a transition between two liquid crystalline mesophases. The low molar mass sample of F3-PPT-CH_3 (M_w = 11 kg mol^{-1}) did not have a detectable T_2 transition, although an endotherm was detected in the high molar mass sample (M_w = 77 kg mol^{-1}) near $T_2 \approx 30$ °C. The measured glass transition temperatures (T_g) of F3-PPT-H and F3-PPT-CH_3 were each 8 ± 2 °C, based on the midpoint of the inflections observed. F3-PPT-H therefore had a substantially larger temperature range between T_g and T_i (≈122 °C) compared to F3-PPT-CH_3 (≈64 °C). The depression of T_i with increasing substituent size is well-known in main-chain LCP[29−31] and is thought to arise from decreasing the length:diameter ratio and linearity of the mesogens.[12,32] The low molar mass and high molar mass samples of F3-PPT-CH_3 had the same value of T_i within experimental uncertainties.

Optical textures in fractionated linear polymers were characterized by polarized light optical microscopy (POM). (Enlarged color versions of all micrographs are presented in the Supporting Information.) After quick cooling from the isotropic melt to any temperature below T_i, both F3-PPT-H and F3-PPT-CH_3 developed a dense threaded texture with numerous intertwining disclinations (Figure 4a). Slow ramp-cooling (2 °C/h) from the melt produced either schlieren textures with dark brushes emanating from point singularities (Figure 4b,d,e) or "domain" textures (Figure 4c,e). Schlieren and domain textures could be observed in different regions within the same sample due to local differences in thickness and/or orientation.

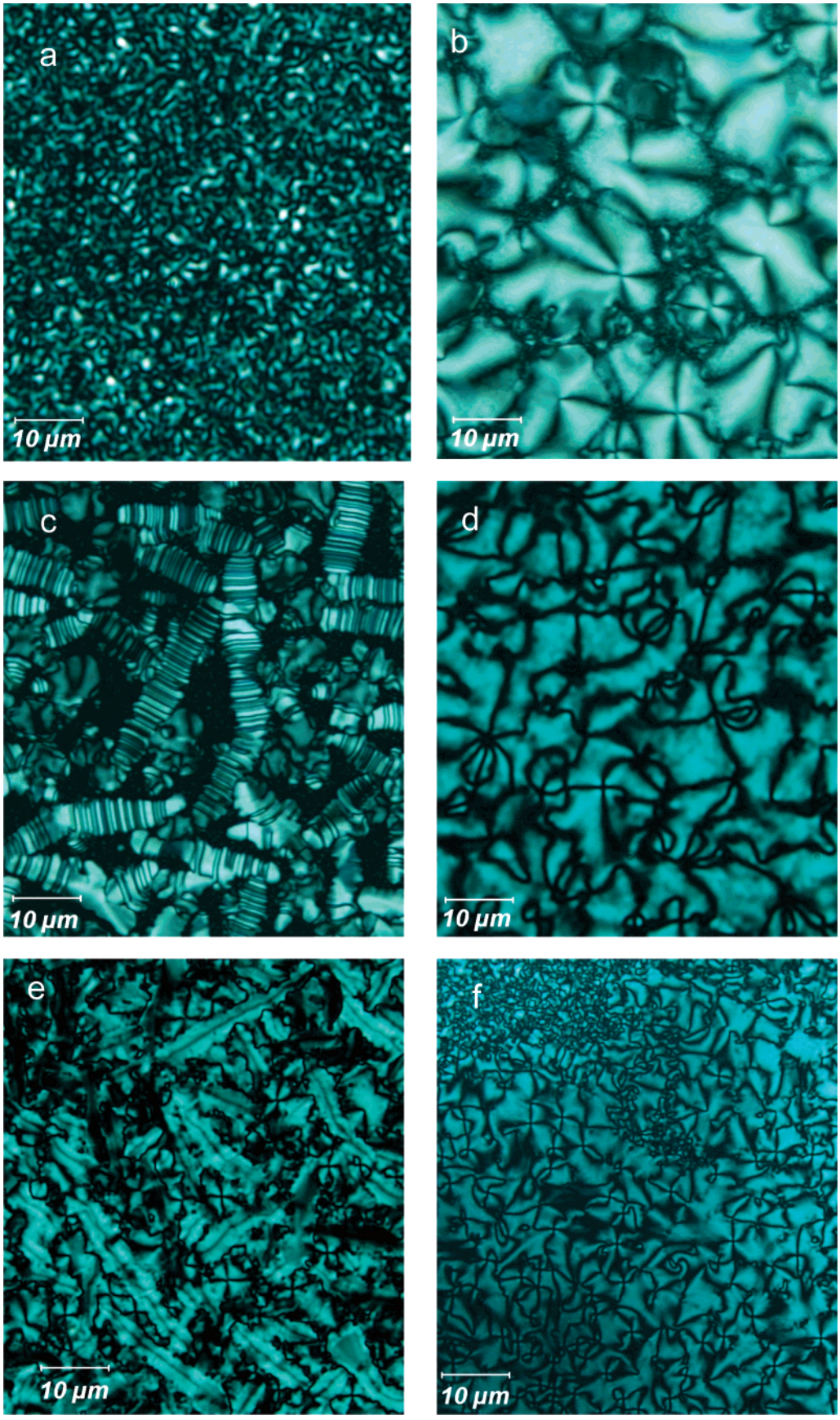

Figure 4. Polarized light optical micrographs of (a) threaded texture in F3-PPT-H (M_w = 85 kg mol^{-1}) quickly cooled to 100 °C from the melt; (b) schlieren texture in F3-PPT-H cooled to 100 °C at 2 °C/h from the melt; (c) "caterpillar" domain texture in F3-PPT-H at 22 °C; (d) schlieren texture in F3-PPT-CH_3 (M_w = 11 kg mol^{-1}) cooled at 2 °C/h to 50 °C from the melt; (e) domain texture in F3-PPT-CH_3 (M_w = 11 kg mol^{-1}) at 22 °C; (f) schlieren and threaded textures in F3-PPT-CH_3 (M_w = 77 kg mol^{-1}) at 22 °C.

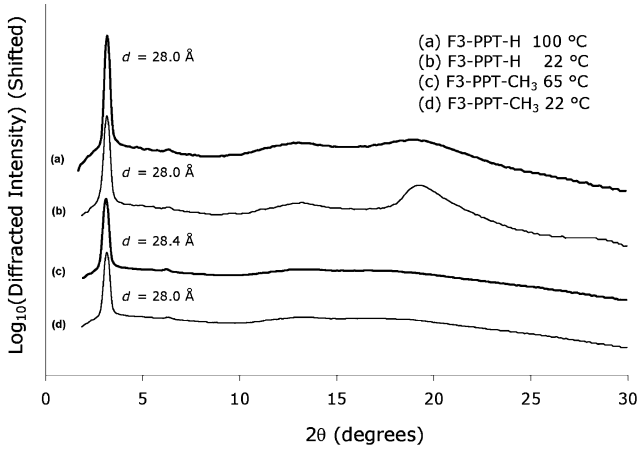

Figure 5. Diffracted X-ray intensity vs 2θ for unoriented F3-PPT-H ($M_w = 85$ kg mol^{-1}) and F3-PPT-CH$_3$ ($M_w = 77$ kg mol^{-1}) above and below their respective T_2 temperatures.

The defect textures formed above T_2 persisted upon cooling below T_2, with only subtle changes in birefringence colors.

Schlieren textures can signify either nematic or smectic ordering, and distinguishing between these phases requires closer examination of the singularities observed, in addition to information from X-ray diffraction. Figure 4d,f depicts point singularities having 2, 4, 6, or 8 dark brushes in F3-PPT-CH$_3$ samples of low and high molar mass. The presence of numerous singularities having more than four brushes is not expected for a nematic phase,[33] as the defect energy scales as s^2, where s is the strength of the singularity, equal to (1/4)(number of brushes).[33] (We note that Zhou et al. have observed high-strength disclinations in nematic polymers with "two-dimensional" mesogens, however.[34,35]) Figure 4b shows the schlieren texture in F3-PPT-H, where point singularities have predominantly two or four brushes. The S_C phase can be ruled out in both F3-PPT-H and F3-PPT-CH$_3$, as the S_C schlieren texture exhibits singularities with exclusively four brushes.[36,37] The S_A phase also seems unlikely, as broken fan or homeotropic textures are normally observed.[36,37] There are at least two known smectic phases that exhibit textures consistent with Figure 5a,b. One possibility is the S_{CA} phase, a layered mesophase in which mesogens in adjacent layers tilt in an alternating sense with respect to the layer normals. The S_{CA} phase has been identified in both low molar mass liquid crystals[38−40] and main-chain thermotropic polyesters,[41−47] and its schlieren texture exhibits singularities having both two and four brushes. Tokita and Watanabe have recently discussed the nature of defects associated with the two-brush ($s = \pm 1/2$) singularities in S_{CA}, main-chain polyesters.[47] A second possibility is the biaxial smectic A (S_{Ab}) phase, which may be indistinguishable from the S_{CA} phase by POM.[48] However, S_{Ab} ordering seems unlikely, as it is rarely found in polymers,[49] and is usually associated with bent-core mesogens in low molar mass liquid crystals.[48,50−52]

The "domain" textures in F3-PPT-H (Figure 4c) and F3-PPT-CH$_3$ (Figure 4e), which are stable both above and below the respective T_2 transition temperatures, suggest smectic ordering rather than nematic. The sharply focused, dark boundaries of the domains are not consistent with nematic textures. The elongated domains in F3-PPT-CH$_3$ exhibit faint, zero-birefringence lines through their approximate midsections at room temperature (Figure 4e). Upon rotation of the sample stage, an elongated domain passes through extinction positions when the long axis of the domain is parallel to either the polarizer or the analyzer, indicating that the optic axis of the domain is equivalent to its long dimension. It is possible that the domains and the four-brush defects in Figure 4e are the same defect structures observed with different orientations. The four-brush singularities may correspond to domains that are oriented with the optic axis perpendicular to the glass slide, whereas the elongated domains could be similar structures having parallel alignment. A markedly different domain texture was observed in F3-PPT−H, especially in thinner regions of the sample, which we named the "caterpillar" texture (Figure 5d). This texture was characterized by elongated domains, some of which developed numerous transverse dark bands upon cooling. The alternating dark and light bands indicate different orientations of the director with respect to the substrate, with dark bands corresponding to perpendicular alignment. The mechanism of formation of the caterpillar domains and the details of their molecular-level organization merit further investigation.

F3-PPT-H and F3-PPT-CH$_3$ samples were also characterized in bulk by WAXD at different temperatures. WAXD measurements on unoriented linear polymers (Figure 5) were first conducted at room temperature, which is below the T_2 transition of each polymer. Both polymers exhibited a low-angle Bragg peak, centered at $2\theta = 3.16°$ ($d = 28.0$ Å) for F3-PPT-H and at $2\theta = 3.15°$ ($d = 28.0$ Å) for F3-PPT-CH$_3$. (Note the log-(intensity) scale in Figure 5.) The presence of a low-angle Bragg peak indicates well-defined positional ordering (layering), so the mesophases occurring below T_2 are smectic. Besides the layering peak, a weak second-order reflection and two diffuse halos at wide angles were observed in each polymer at 22 °C (halos centered at approximately $2\theta \approx 13.5°$, 19.5° for F3-PPT-H and $2\theta \approx 13.5°$, 17.5° for F3-PPT-CH$_3$). The presence of two diffuse halos indicates that there are two separate characteristic spacings between the mesogens within smectic layers. Figure 5 also compares the diffracted intensity in the low-angle region for F3-PPT-H and F3-PPT-CH$_3$ at different temperatures above and below their respective T_2 transitions. In both cases, the strong layering reflection is still present above T_2, confirming that the mesophases above T_2 are also smectic phases. Above T_2, the d-spacing increases only slightly for F3-PPT-CH$_3$ and remains about the same for F3-PPT-H, whereas the wide-angle halos weaken somewhat and broaden, especially for F3-PPT-H. These changes indicates that mesogens gain rotational and/or translational degrees of freedom within the smectic layers above T_2, with relatively little change in interlayer spacing.

Oriented samples of linear polymers were drawn in the smectic state (refer to Experimental Section) and characterized by WAXD. Figure 6 shows integrated intensity vs azimuthal angle (χ) for the low-angle reflection (integrated over $2.5° \leq 2\theta \leq 3.8°$) and the outer wide-angle halo (integrated over $18° \leq 2\theta \leq 22°$) for F3-PPT-H. Well-defined maxima are observed in the low-angle reflection at $\chi = -90°$ and 90°. The wide-angle halo exhibits four weak maxima at approximately $\chi = -45°$, 45°, 135°, and 225°. This diffraction pattern is consistent with a S_{CA} phase having a "bookshelf" arrangement of layers, in which the smectic layer normals are predominantly oriented perpendicular to the axis of extension, and mesogens are tilted by about 45°.

A schematic diagram of the oriented mesophase in F3-PPT-H is shown in Figure 7. The chain axis is presumed to be parallel to the layer normals, with the zigzag tilting of mesogens in adjacent layers that characterizes the S_{CA} state. This model requires the supposition that the chain axes are aligned predominantly perpendicular to the axis of elongation after stretching. However, this "anomalous" alignment of smectic layer normals perpendicular to the axis of elongation is not

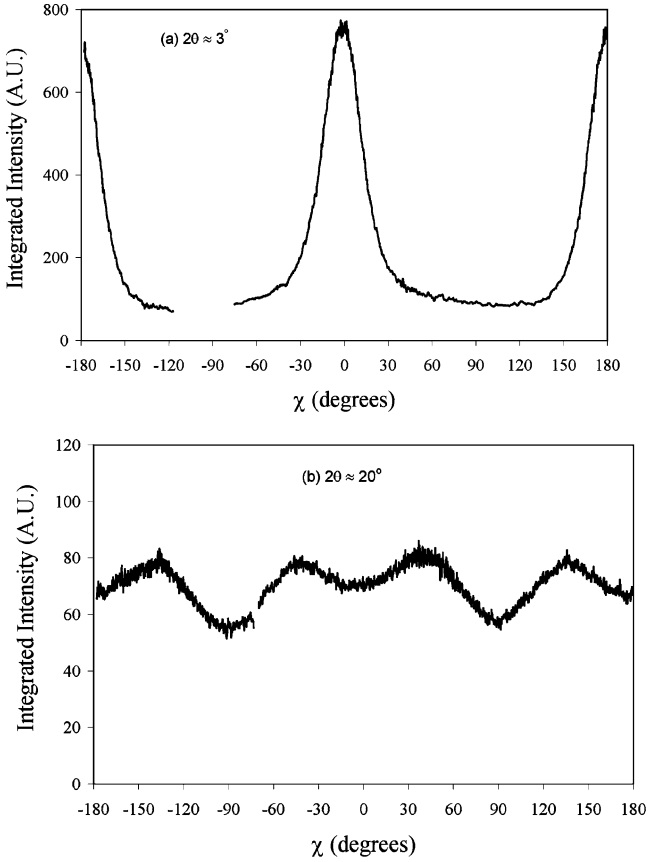

Figure 6. Diffracted X-ray intensity vs azimuthal angle (χ) at 22 °C for uniaxially drawn F3-PPT-H linear polymer. The axis of extension lies along $\chi = (0°, 180°)$. (a) Intensity of low-angle reflection integrated over ($2.7° \leq 2\theta \leq 3.7°$). (b) Intensity of wide-angle halo integrated over ($18° \leq 2\theta \leq 22°$). Data near/behind beamstop are omitted for clarity.

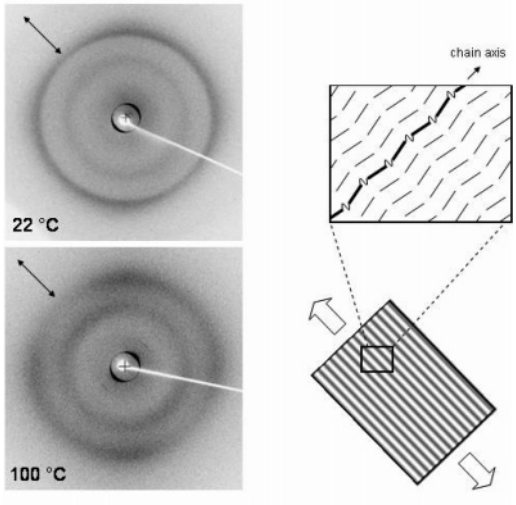

Figure 7. Diffraction patterns at two temperatures and illustration of S_{CA} ordering with anomalous layer orientation in uniaxially drawn F3-PPT-H. Double-ended arrows designate the axis of extension.

unusual for drawn smectic main-chain LCP,[42−46,53−55] including those that form a S_{CA} phase.[44,45,56] Watanabe et al. suggest that the alignment of the chain axes perpendicular to the axis of elongation could indicate the formation of smectic domains, in which irregular chain folding (hairpin formation) occurs.[56] The domains are thought to slide past one another during elongation, such that their long dimension is aligned with the axis of elongation, while the layer normals (and chain axes) assume

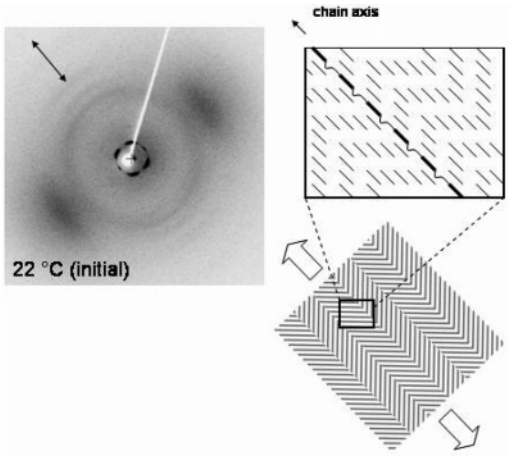

Figure 8. Diffraction pattern for oriented F3-PPT-CH_3 ($M_w = 77$ kg mol^{-1}) immediately after uniaxial drawing at 22 °C and illustration of buckled layer arrangement.

the perpendicular orientation. The development of normal (parallel) alignment vs anomalous (perpendicular) alignment of smectic layer normals with respect to the drawing direction is known to depend on both the strain rate and temperature.[42−46,55] We did not attempt to control the strain rate in this study, but the anomalous layer alignment was always obtained for F3-PPT-H under the conditions employed.

Figure 7 also compares diffraction patterns for drawn F3-PPT-H at temperatures above and below its T_2 transition (52 °C). All intensity maxima noted at 22 °C are still present at 100 °C, but the wide-angle halos are significantly broadened at 100 °C. Little change in the tilt angle of the mesogens, if any, is seen upon passing T_2, and changes in the interlayer *d*-spacings are also minimal. On the basis of this evidence, and recalling that the optical textures observed by POM were nearly indistinguishable above and below T_2, we concluded that the phase below T_2 is a higher order smectic state that is structurally similar to the S_{CA} phase. The T_2 transition therefore appears to represent a significant change in chain dynamics rather than a structural transformation. Chains may undergo a reduction in conformational entropy upon cooling below T_2, as mesogens lose rotational and/or translational degrees of freedom, while the layered structure of the S_{CA} mesophase is essentially preserved.

The flow alignment observed in drawn F3-PPT-CH_3 ($M_w = 77$ kg mol^{-1}) was markedly different (Figure 8). Judging by the wide-angle halo, the mesogens are aligned with the axis of elongation, but smectic layer normals are tilted. The separation of the low-angle reflection into four sharp maxima may indicate development of buckling instabilities in the layers similar to those observed in strained S_A liquid crystals[57−59] and strained monodomain S_A elastomers.[17] (The schematic illustration in Figure 8 may be somewhat oversimplified, as buckling instabilities may also generate some regions with disrupted ordering.[17]) The diffraction pattern observed in oriented F3-PPT-CH_3 immediately after stretching was transient, relaxing over a period of several days at 22 °C to yield a new pattern consistent with a S_{CA} phase having the bookshelf arrangement of layers (Figure 9). Figure 10a depicts the convergence of the four maxima in the inner layering reflection to two peaks centered at ($\chi = 0°$, 180°) after 16 days of relaxation at 22 °C. Figure 10b illustrates the simultaneous resolution of the outer halo into four overlapping maxima after 16 days due to tilting of mesogens with respect to the original axis of elongation. The azimuthal intensity distribution in Figure 10b (bottom curve) could be fit satisfac-

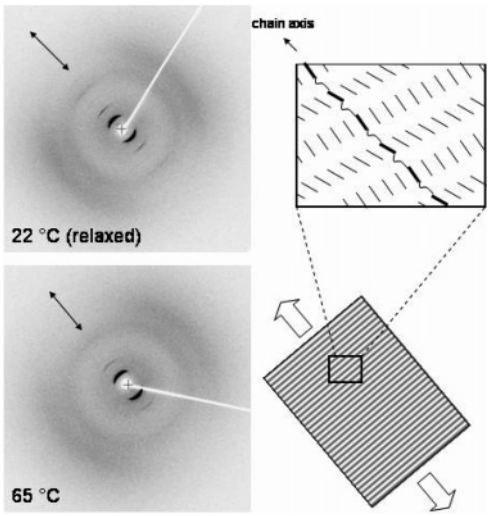

Figure 9. Observed diffraction patterns and illustration of S_{CA} ordering with "bookshelf" layering in oriented F3-PPT-CH_3 (M_w = 77 kg mol^{-1}) 16 days after stretching at 22 °C and after heating the same to 65 °C. Double-ended arrows designate the axis of extension.

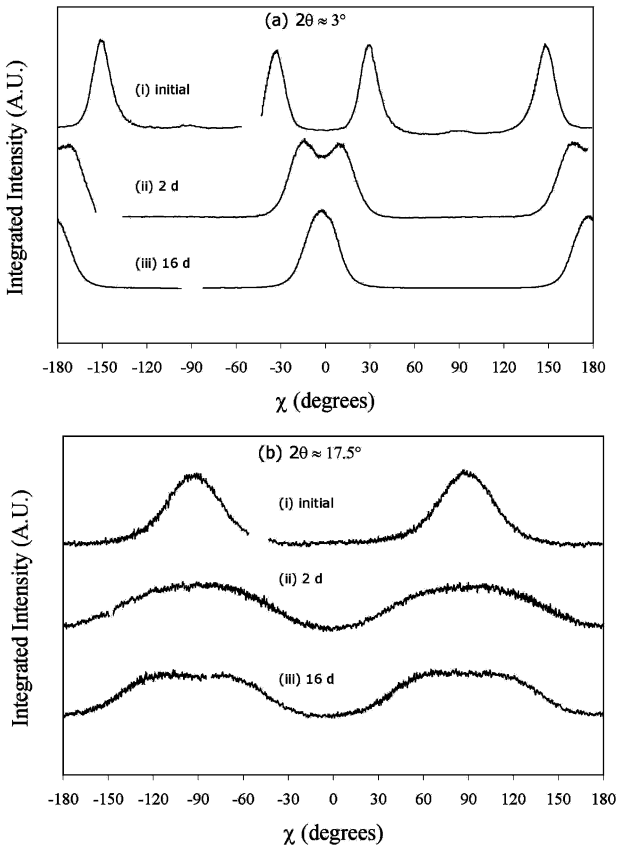

Figure 10. Integrated intensity vs azimuthal angle (χ) for F3-PPT-CH_3 (M_w = 77 kg mol^{-1}) at 22 °C immediately after stretching, after 2 days relaxation, and after 16 days relaxation. Top: low-angle reflection integrated over (2.5° ≤ 2θ ≤ 3.8°). Bottom: wide-angle reflection integrated over (16° ≤ 2θ ≤ 19°). The axis of extension lies along χ = (0°, 180°). Data near/behind beamstop are omitted for clarity. Data were rescaled by an arbitrary constant and shifted for ease in comparing line shapes.

torily to a sum of two Lorentzian functions and a constant background (Supporting Information). The center positions of the fitted Lorentzian functions indicate a mesogen tilt angle of ~25° with respect to the layer normals (in the relaxed state).

A proposed model for the structure of the oriented S_{CA} mesophase in F3-PPT-CH_3 (after relaxation) is presented in

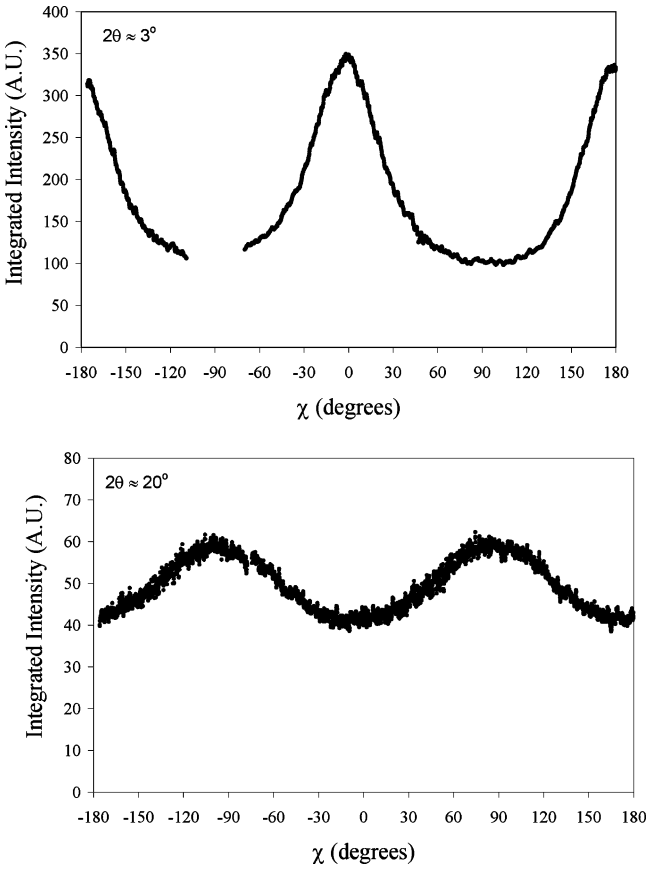

Figure 11. WAXD data at 22 °C for uniaxially drawn elastomer E-H (L/L_0 = 2.3). (a) Low-angle reflection integrated over (2.3° ≤ 2θ ≤ 3.8°). (b) Wide-angle halo integrated over (18° ≤ 2θ ≤ 22°). Data near/behind beamstop are omitted for clarity. The axis of extension lies along χ = (0°, 180°).

Figure 9. The chain axes are oriented in the direction of flow, judging by the positions of the maxima in the low-angle layering reflection. The parallel alignment of smectic layer normals was always observed in F3-PPT-CH_3, whereas the perpendicular alignment was always observed in F3-PPT-H under the drawing conditions employed here. Although our samples were drawn manually without controlling the strain rate, the orientations observed were repeatable after multiple measurements under similar conditions.

It is interesting to compare the thermal behavior of F3-PPT-H to the similar linear polymer having unsubstituted BHQ-type mesogens, first characterized by Ringsdorf et al. in 1983 (structure 3a in ref 9),[9] which differs only in the reversal of the ester bridges of the mesogens. The two polymers have virtually identical values of T_i, while Ringsdorf reports a crystallization endotherm at 35 °C that may be similar to our T_2 reported at 52 °C. Unfortunately, the glass transition temperature of the polymer with BHQ-type mesogens and the nature of its smectic ordering are not characterized in ref 9.

3.2. Smectic Elastomers. Cross-linked MCLCE were prepared from both PPT-H and PPT-CH_3 mesogens by an "A_2 + B_2 + A_4" nonlinear polycondensation, with B_2 ≡ mesogen, A_2 ≡ F3, and A_4 ≡ tetrakis(dimethylsiloxy)silane. Procedures for optimization of elastomer synthesis (variation of stoichiometric parameters r and ρ) and removal of solubles by extraction are presented in the Experimental Section. The optimal elastomer prepared from PPT-H mesogen with ρ = 0.08 and r = 1.50 was designated E-H, and the elastomer prepared from PPT-CH_3 mesogen with ρ = 0.08 and r = 1.36 was designated E-CH_3. Both elastomers were smectic and exhibited a low-angle

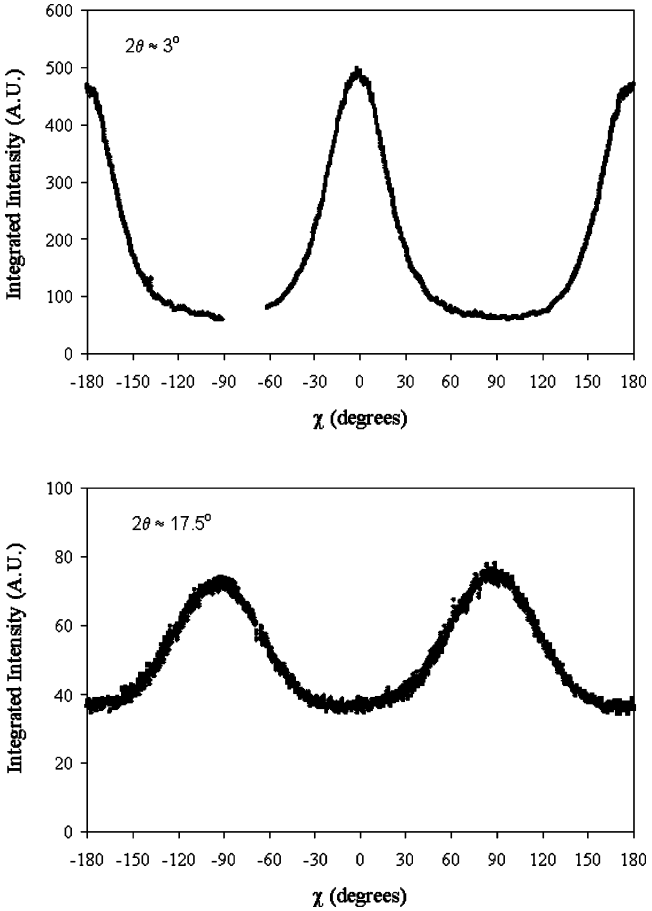

Figure 12. WAXD data at 22 °C for uniaxially drawn elastomer E-CH_3 ($L/L_0 = 2.0$). (a) Low-angle reflection integrated over ($2.5° \leq 2\theta \leq 3.8°$). (b) Wide-angle reflection integrated over ($16° \leq 2\theta \leq 19°$). Data near/behind beamstop are omitted for clarity. The axis of extension lies along $\chi = (0°, 180°)$.

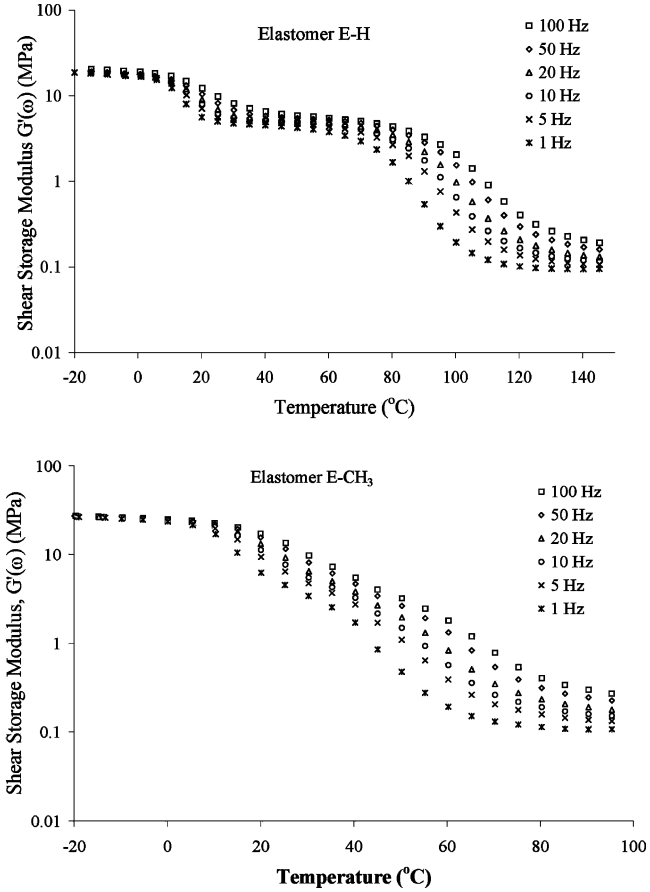

Figure 13. Temperature dependence of storage moduli for elastomers E-H and E-CH_3 measured in oscillatory shear.

Bragg peak at $2\theta \approx 2.9°$ in both the unperturbed state and under uniaxial tension. Calculated *d*-spacings for the low-angle reflection were 31.4 ± 1.0 Å for E-H and 30.5 ± 1.0 E-CH_3, slightly larger than the values for the respective linear polymers. DSC traces for E-H and E-CH_3 were nearly featureless, except for the inflection at $T_g \approx 10$ °C, despite clear evidence of smectic ordering from WAXD and DMA.

Elastomers were characterized by WAXD in the aligned state under uniaxial tension. The extension ratio ($\lambda = L/L_0$) was 2.3 for E-H and 2.0 for E-CH_3. Figures 11 and 12 present integrated azimuthal intensity plots for the low-angle reflections and the diffuse outer halos in E-H and E-CH_3, respectively. Judging by the low-angle reflections, the layer normals are parallel to the axis of extension in both elastomers, suggesting that the backbones of the elastic chains align predominantly in the direction of extension. In E-H, the smectic layer normals are therefore oriented 90° away from the orientation observed in the drawn linear polymer (under the limited range of drawing conditions studied). No evidence of layer buckling was found for E-CH_3, unlike the linear F3-PPT-CH_3.

The diffraction patterns observed for E-H and E-CH_3 are consistent with smectic ordering, but the azimuthal intensity distributions in the wide-angle halos differ from those observed in the drawn linear polymers. At a glance, the observed diffraction patterns (Figures 11 and 12) suggest S_A ordering, judging by the apparent unimodal maxima in the wide-angle halo at $\chi = -90°, +90°$. However, the diffraction patterns in Figures 11 and 12 could also be consistent with S_{CA} ordering with a low mesogen tilt angle. Bello et al. also observed diffraction patterns that easily could be mistakenly assigned to a S_A phase in a drawn S_{CA} MCLCP, for certain conditions of temperature and strain rate.[44] In a stretched MCLCE, one must also consider that the applied uniaxial tension may affect the preferred conformation of the elastic chains, altering the tilt angle of the mesogens and/or the arrangement of layers. Thus, it seems reasonable that the elastomers could also exhibit S_{CA} ordering in the unperturbed state, like the linear polymers, although the tilt angle may not be the same, recalling the slightly higher *d*-spacings in the elastomers.

E-H and E-CH_3 were characterized by dynamic mechanical analysis (DMA) in small-strain, oscillatory shear (Figure 13). In DMA heating ramps, a sharp drop in the shear storage modulus was observed slightly above the glass transition temperature (≈10 °C) measured by DSC. Upon further heating, a second drop in the storage modulus was observed in each elastomer due to the disappearance of the smectic phase. E-H clearly has a broader temperature range of smectic ordering than E-CH_3, consistent with the behavior of the linear polymers. No direct evidence of a T_2 transition was found in either elastomer. It is possible that the presence of some short chains and/or the incorporation of branched A_4 units suppresses the T_2 transition to lower temperatures.

Figure 14 shows the temperature dependence of the loss tangent ($\tan \delta \equiv G''\omega)/G'(\omega)$) for E-H and E-$CH_3$, measured at frequencies of $\omega = 1$ and 100 Hz. Loss tangents for both elastomers exhibit the usual maxima associated with the glass transition, which shifts to higher temperatures as frequency increases. In addition, a more pronounced loss peak is observed at higher temperature, with maximum values of $\tan \delta \approx 1.0$ for

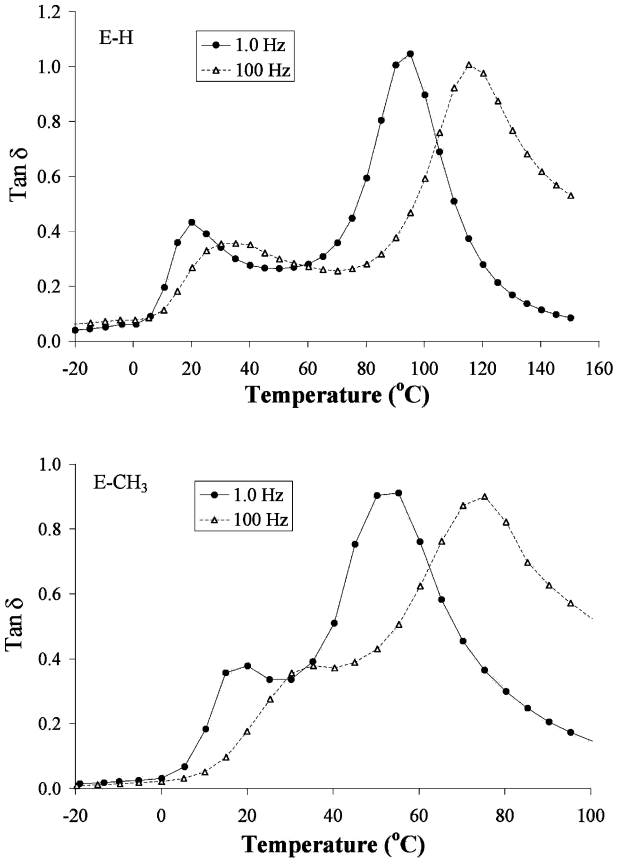

Figure 14. Temperature dependence of mechanical loss factor for elastomers E-H and E-CH_3 in oscillatory shear at $\omega = 1$ and 100 Hz. Lines are a guide to the eye.

E-H and tan $\delta \approx 0.9$ for E-CH_3. A strong maximum in tan δ near the clearing temperature has also been noted by Weilepp et al.[61] in polydomain S_A side-chain LCE. In both the present study and in ref 61, the temperature at which the maximum loss occurs corresponds to the region of steepest decline in the storage modulus, which has previously been dubbed the "transition" or "pretransformational" region.[61,62] The high damping may arise from relaxation of the smectic microstructure on a time scale of order $1/\omega$, corresponding to continuous breaking and re-forming of smectic layers in response to the applied deformation. However, the physical origin of the high mechanical loss is open to question without a precise determination of the changes in mesomorphic ordering occurring within the transition region. The peak in tan δ shifts to higher temperatures for higher frequencies of observation, which is consistent with the observations of Weilepp et al.[61] for S_A side-chain LCE. Interestingly, in earlier studies by Clarke et al.[4] and Gallani et al.[60] concerning side-chain LCE that pass through a stable nematic state prior to clearing, little or no loss peak was observed at the smectic−nematic phase boundary. Thus, it seems unlikely that the loss peak observed in the transition region for our MCLCE can be attributed to formation of a transient nematic state in the transition region, especially since no stable nematic phase was found in the linear polymers at any temperature.

4. Summary and Conclusions

PPT units are versatile structural units for preparation of main-chain siloxane polymers and elastomers with low-temperature smectic mesophases. F3-PPT-H and F3-PPT-CH_3 linear polymers form S_{CA} phases below their respective clearing temperatures. A higher order smectic phase with similar interlayer *d*-spacing is observed upon cooling below a temperature T_2. The defect texture observed in the optical microscope in the S_{CA} phase is retained upon cooling below T_2, with minimal changes in the interlayer *d*-spacings. For the elastomers, evidence from DMA and WAXD characterizes the mesophase as a smectic phase with slightly larger interlayer *d*-spacing than that found in the linear polymers.

The high values of tan δ noted in smectic MCLCE point to their possible use as vibration damping materials. Clarke et al. have previously noted the exceptional damping characteristics of nematic and smectic side-chain LCE, although they identified the nematic state as a better damping phase than the smectic.[4] Whereas nematic elastomers can exhibit high mechanical damping over the entire temperature range of nematic ordering, the smectic elastomers studied so far exhibit a pronounced loss peak over a comparatively narrow temperature range near the clearing transition. Ring substitution of the mesogens therefore represents a simple synthetic approach for "tuning" the dynamic mechanical response of smectic MCLCE to selectively damp vibrations over a comparatively narrow temperature/frequency range for possible vibration isolation applications. In addition, the "mixed mesogen" copolymerization approach described by Mather et al.[18] could be applied to further manipulate the clearing temperature. The ($A_2 + B_2 + A_4$) nonlinear polymerization technique also provides a basis to influence the dynamic mechanical response by systematically varying the cross-link density and the perfection of the network structure, important variables that must be considered in future work.

Acknowledgment. We thank Mark Angelone for help with the WAXD experiments and Dr. Sachin Borkar for assistance in performing GPC characterization. We thank Ralph Colby of Penn State University and Oleg Lavrentovich of Kent State University for helpful discussions.

Supporting Information Available: Enlarged color micrographs from Figure 4a−f; curve-fitting of X-ray line shape in Figure 10b (bottom curve: 16 days) to sum of two identical Lorentzian functions. This material is available free of charge via the Internet at http//pubs.acs.org.

References and Notes

(1) Larson, R. G. *The Structure and Rheology of Complex Fluids*; Oxford University Press: New York, 1999.
(2) Warner, M.; Terentjev, E. M. *Liquid Crystal Elastomers*; Clarendon Press: Oxford, 2003.
(3) Clarke, S. M.; Hotta, A.; Tajbakhsh, A. R.; Terentjev, E. M. *Phys. Rev. E* **2002**, *65*, 021804 1−6.
(4) Clarke, S. M.; Tajbakhsh, A. R.; Terentjev, E. M.; Remillat, C.; Tomlinson, G. R.; House, J. R. *J. Appl. Phys.* **2001**, *89*, 6530−6535.
(5) Thomsen, D. L.; Keller, P.; Naciri, J.; Pink, R.; Jeon, H.; Shenoy, D.; Ratna, B. R. *Macromolecules* **2001**, *34*, 5868−5875.
(6) Spillmann, C. A.; Naciri, J.; Martin, B. D.; Farahat, W.; Herr, H.; Ratna, B. R. *Sens. Actuators, A* **2007**, *133*, 500−505.
(7) Spillmann, C. M.; Ratna, B. R.; Naciri, J. *Appl. Phys. Lett.* **2007**, *90*.
(8) Spillmann, C. M.; Naciri, J.; Chen, M. S.; Srinivasan, A.; Ratna, B. R. *Liq. Cryst.* **2006**, *33*, 373−380.
(9) Aguilera, C.; Bartulin, J.; Hisgen, B.; Ringsdorf, H. *Makromol. Chem.* **1983**, *184*, 253−262.
(10) Aguilera, C.; Ringsdorf, H. *Polym. Bull. (Berlin)* **1984**, *12*, 93−98.
(11) Braun, F.; Willner, L.; Hess, M.; Kosfeld, R. *Makromol. Chem.* **1990**, *191*, 1775−1785.
(12) Costa, G.; Nora, A.; Trefiletti, V.; Valenti, B. *Mol. Cryst. Liq. Cryst.* **1988**, *157*, 79−95.
(13) Diaz, F.; Tagle, L. H.; Valdebenito, N.; Aguilera, C. *Polymer* **1993**, *34*, 418−422.
(14) Donnio, B.; Wermter, H.; Finkelmann, H. *Macromolecules* **2000**, *33*, 7724−7729.
(15) Horn, M.; Hepuzer, Y.; Yagci, Y.; Bilgin-Eran, B.; Cernenco, U.; Harabagiu, V.; Pinteala, M.; Simionescu, B. C. *Eur. Polym. J.* **2002**, *38*, 2197−2205.

(16) Hiraoka, K.; Uematsu, Y.; Stein, P.; Finkelmann, H. *Macromol. Chem. Phys.* **2002**, *203*, 2205−2210.
(17) Nishikawa, E.; Finkelmann, H. *Macromol. Chem. Phys.* **1999**, *200*, 312−322.
(18) Rousseau, I. A.; Qin, H. H.; Mather, P. T. *Macromolecules* **2005**, *38*, 4103−4113.
(19) Clarke, S. M.; Hotta, A.; Tajbakhsh, A. R.; Terentjev, E. M. *Phys. Rev. E* **2001**, *64*, 1−8.
(20) Hotta, A.; Terentjev, E. M. *Eur. Phys. J. E* **2003**, *10*, 291−301.
(21) Bergmann, G. H. F.; Finkelmann, H.; Percec, V.; Zhao, M. Y. *Macromol. Rapid Commun.* **1997**, *18*, 353−360.
(22) Sacripante, G.; Ober, C. K.; Bluhm, T.; Panettoni, M.; Alexandru, L. *J. Polym. Sci., Polym. Chem.* **1995**, *33*, 1913−1916.
(23) Barclay, G. G.; Ober, C. K.; Papathomas, K. I.; Wang, D. W. *Macromolecules* **1992**, *25*, 2947−2954.
(24) Costa, G.; Nora, A.; Trefiletti, V.; Valenti, B. *Mol. Cryst. Liq. Cryst.* **1988**, *157*, 79−95.
(25) Dewar, M. J. S.; Riddle, R. M. *J. Am. Chem. Soc.* **1975**, *97*, 6658−6662.
(26) Patel, S. K.; Malone, S.; Cohen, C.; Gillmor, J. R.; Colby, R. H. *Macromolecules* **1992**, *25*, 5241−5251.
(27) Hedden, R. C.; Saxena, H.; Cohen, C. *Macromolecules* **2000**, *33*, 8676−8684.
(28) Gilra, N.; Cohen, C.; Panagiotopoulos, A. Z. *J. Chem. Phys.* **2000**, *112*, 6910−6916.
(29) Antoun, S.; Lenz, R. W.; Jin, J. I. *J. Polym. Sci., Polym. Chem.* **1981**, *19*, 1901−1920.
(30) Zhun, Q.; Lenz, R.; Jin, J.-I. *Polymeric Liquid Crystals*; Plenum Press: New York, 1984.
(31) Sacripante, G.; Ober, C. K.; Bluhm, T.; Panettoni, M.; Alexandru, L. *J. Polym. Sci., Polym. Chem.* **1995**, 1913−1916.
(32) Jin, J. I.; Kang, C. S. *Polymer* **1993**, *34*, 2407−2412.
(33) Nehring, J.; Saupe, A. *J. Chem. Soc., Faraday Trans. 2* **1972**, *68*, 1−15.
(34) Zhou, Q. F.; Wu, Z. C.; Lenz, R. W. *Polym. Bull. (Berlin)* **1991**, *27*, 257−260.
(35) Zhou, Q. F.; Wan, X. H.; Zhang, F.; Zhang, D.; Wu, Z. C.; Feng, X. D. *Liq. Cryst.* **1993**, *13*, 851−858.
(36) Gray, G. W.; Goodby, J. W. G. *Smectic Liquid Crystals*; Leonard Hill: Glasgow, 1984.
(37) Zhou, Q.-F.; Wang, X.-J. *Liquid Crystlline Polymers*; World Scientific: Singapore, 2004.
(38) Niori, T.; Adachi, S.; Watanabe, J. *Liq. Cryst.* **1995**, *19*, 139−148.
(39) Takanishi, Y.; Takezoe, H.; Fukuda, A.; Watanabe, J. *Phys. Rev. B* **1992**, *45*, 7684−7689.
(40) Takanishi, Y.; Takezoe, H.; Fukuda, A.; Komura, H.; Watanabe, J. *J. Mater. Chem.* **1992**, *2*, 71−73.
(41) Tokita, M.; Osada, K.; Watanabe, J. *Liq. Cryst.* **1998**, *24*, 477−480.
(42) Bello, P.; Bello, A.; Riande, E.; Heaton, N. J. *Macromolecules* **2001**, *34*, 181−186.
(43) Bello, P.; Bello, A.; Lorenzo, V. *Polymer* **2001**, *42*, 4449−4452.
(44) Martinez-Gomez, A.; Perena, J. M.; Lorenzo, V.; Bello, A.; Perez, E. *Macromolecules* **2003**, *36*, 5798−5803.
(45) Tokita, M.; Tokunaga, K.; Funaoka, S.; Osada, K.; Watanabe, J. *Macromolecules* **2004**, *37*, 2527−2531.
(46) Osada, K.; Koike, M.; Tagawa, H.; Hunaoka, S.; Tokita, M.; Watanabe, J. *Macromolecules* **2005**, *38*, 7337−7342.
(47) Tokita, M.; Watanabe, J. *Polym. J.* **2006**, *38*, 611−638.
(48) Smalyukh, I. I.; Pratibha, R.; Madhusudana, N. V.; Lavrentovich, O. D. *Eur. Phys. J. E* **2005**, *16*, 179−191.
(49) Leube, H. F.; Finkelmann, H. *Makromol. Chem.* **1991**, *192*, 1317−1328.
(50) Pratibha, R.; Madhusudana, N. V.; Sadashiva, B. K. *Science* **2000**, *288*, 2184.
(51) Sadashiva, B. K.; Reddy, R. A.; Pratibha, R.; Madhusudana, N. V. *Chem. Commun.* **2001**, 2140−2141.
(52) Reddy, R. A.; Sadashiva, B. K. *J. Mater. Chem.* **2004**, *14*, 310−319.
(53) Leland, M.; Wu, Z. Q.; Chhajer, M.; Ho, R. M.; Cheng, S. Z. D.; Keller, A.; Kricheldorf, H. R. *Macromolecules* **1997**, *30*, 5249−5254.
(54) Tokita, M.; Osada, K.; Kawauchi, S.; Watanabe, J. *Polym. J.* **1998**, *30*, 687−690.
(55) Fernandez-Blazquez, J. P.; Bello, A.; Perez, E. *Macromolecules* **2007**, *40*, 703−709.
(56) Tokita, M.; Osada, K.; Watanabe, J. *Liq. Cryst.* **1997**, *23*, 453−456.
(57) de Gennes, P. G.; Prost, J. *The Physics of Liquid Crystals*; Clarendon Press: Oxford, 1993.
(58) Delaye, M.; Ribotta, R.; Durand, G. *Phys. Lett. A* **1973**, *A 44*, 139−140.
(59) Clark, N. A.; Meyer, R. B. *Appl. Phys. Lett.* **1973**, *22*, 493−494.
(60) Gallani, J. L.; Hilliou, L.; Martinoty, P.; Doublet, F.; Mauzac, M. *J. Phys. II* **1996**, *6*, 443−452.
(61) Weilepp, J.; Stein, P.; Assfalg, N.; Finkelmann, H.; Martinoty, P.; Brand, H. R. *Europhys. Lett.* **1999**, *47*, 508−514.
(62) Assfalg, N.; Finkelmann, H. *Macromol. Chem. Phys.* **2001**, *202*, 794−800.

MA0706374